Performance Analysis and Power Control of Cell-Free Massive MIMO over Non-Reciprocal Channels

Lirui Luo, Jiayi Zhang, Shuaifei Chen, and Bo Ai

2021 IEEE/CIC International Conference on Communications in China (ICCC) | 978-1-6654-4385-2/21/$31.00 ©2021 IEEE | DOI: 10.1109/ICCC52777.2021.9580402

***Abstract*—In this paper, we investigate the important impacts of imperfect channel state information (CSI) and pilot contamination of cell-free (CF) multiple-input multiple-output (MIMO) systems over non-reciprocal channels with large-scale fading precoding (LSFP). We derive analytical lower bounds of spectral efficiency (SE) for a physically inspired channel non-reciprocity (NRC) model where the NRC variables vary slowly in time. By using our derived closed-form expressions, we study the influence of NRC on the max-min power control scheme. The analysis shows that the achievable downlink SE is only sensitive to the access points (APs) side phase non-reciprocity under pilot contamination and conjugate beamforming, hence the corresponding calibration can be simplified with practical feasibility. Simulation results illustrate that when considering any power control scheme, pilot contamination and NRC both reduce the SE performance while the former shows a greater effect. However, different power control schemes show different sensitivity to NRC. More precisely, the max-min scheme loses its superiority compared to the equal power scheme as the NRC increases. Our results are new and different from the extent CF power control schemes which consider perfect NRC.**

I. Introduction

Cell-free (CF) multiple-input multiple-output (MIMO) is a promising technique for beyond fifth-generation (5G) networks where many randomly distributed access points (APs) jointly serve a much smaller number of spatially multiplexed user equipments (UEs) [1], [2]. CF massive MIMO can provide a much higher coverage than cellular massive MIMO systems due to the random locations between APs and UEs [3]. The large energy efficiency and spectral efficiency (SE) make it competitive to traditional cellular networks [4].

In a time-division duplexing (TDD) CF massive MIMO network, uplink pilots are used to estimate the channel between APs and UEs [3], [5], [6]. Then such information is delivered to the APs to calculate precoding weights for the downlink [7]. Such signal processing is based on channel reciprocity. However, based on the frequency response mismatches on the receivers and transmitters, the effective channels are known to be non-reciprocal while only the physical propagation could be reciprocal, and it is named as TDD-MIMO channel non-reciprocity (NRC) in the literature [8]–[11].

This work was supported in part by National Natural Science Foundation of China under Grant U1834210, in part by ZTE Corporation, and State Key Laboratory of Mobile Network and Mobile Multimedia Technology.

L. Luo, J. Zhang and S. Chen are with the School of Electronic and Information Engineering, Beijing Jiaotong University, Beijing 100044, China.

B. Ai is with the State Key Laboratory of Rail Traffic Control and Safety, Beijing Jiaotong University, Beijing 100044, China.

Recently, the effect of NRC has been initially considered in CF massive MIMO systems [12]–[17]. In [12], [13], the NRC variables are considered constant over many coherence intervals of the propagation channel, due to the operating conditions and the hardware implementation. In [14], NRC is considered in CF massive MIMO with imperfect channel state information (CSI). Moreover, the authors of [15] considered NRC in CF massive MIMO with non-orthogonal multiple access (NOMA). However, the impact of NRC in CF massive MIMO with pilot contamination and imperfect CSI has not been considered. More importantly, the power control considering the effect of NRC is still not discussed in the existing literature. This makes the power control scheme not effective in practice. The max-min power control is well-known for providing good performance gains in CF massive MIMO, thus we analyze it under the case of NRC. Besides, LSFP has been proposed as an efficient method for performance improvement in cellular massive MIMO systems [16], [17], which motivates us to consider it in the CF massive MIMO case. Therefore, the major contributions of this paper are three-fold:

- We derive analytical expressions of the SE lower bounds with perfect and imperfect CSI and pilot contamination based on the physically inspired NRC model, using LSFP to improve the downlink performance.
- Under the proposed SE, we derive that under conjugate beamforming and pilot contamination, the SE is only sensitive to AP-side phase NRC.
- We formulate the max-min power control problem as a series of second-order cone programs (SOCPs) for the downlink of CF massive MIMO and propose a successive algorithm to solve it.

Notations: Boldface letters denote column vectors. The superscripts $()^T$, $()^*$ and $()^H$ denote transpose, conjugate, and conjugate transpose, respectively. The expectation operators and Euclidean norm are denoted by $||\cdot||$ and $\mathbb{E}\{\cdot\}$, respectively. The circularly symmetric complex Gaussian distribution is denoted by $\mathcal{CN}\left(0,\sigma^2\right)$ and real-valued Gaussian distribution is denoted by $\mathcal{N}\left(0,\sigma^2\right)$.

II. System Model

A. Basic Assumptions

We consider a CF massive MIMO system with M single-antenna APs and K single-antenna UEs, where the APs are connected to a central processing unit (CPU) that provides signaling and the payload data needed for synchronized downlink

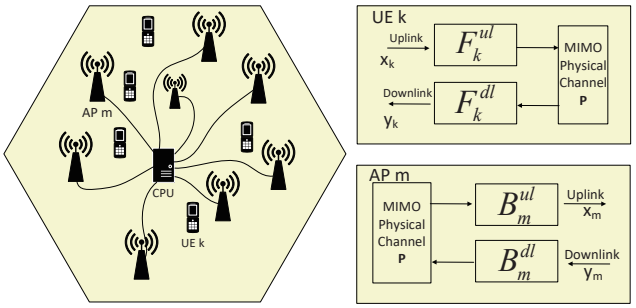

Fig. 1. A CF massive MIMO system over non-reciprocity channels.

transmission via a fronthaul network, (see Fig. 1). We suppose that all K UEs are simultaneously served by all M APs in the same time-frequency resource, while all APs are connected via error-free fronthaul connections.

Based on the TDD principle assumption, each coherence interval is divided into uplink training and downlink data transmission. In the uplink training phase, each UE sends its pilot sequence to the APs then each AP estimates the channels. Such channel estimates are used to precode the downlink payload, and to transmit the uplink signals. We assume the pilots are arbitrarily allocated to the UEs. And the uplink training duration, denoted by τ_p, is less than K. Thus more than one UE is assigned to each pilot. This causes the pilot contamination effect. Also, We focus on the downlink transmission where the APs serve the UEs with the aid of LSFP at the CPU.

B. Non-Reciprocal Channel Modelling

The channels affected by the hardware and the physical propagation, are usually different for the non-ideal elements in the analog circuitries. Similar to [13], [14], [18], we model the effective channels as $\mathbf{G}^{ul} = \mathbf{B}^{ul}\mathbf{P}\mathbf{F}^{ul}$ and $\mathbf{G}^{dl} = \mathbf{B}^{ul}\mathbf{P}^T\mathbf{F}^{dl}$, where $\mathbf{G}^{ul} \in \mathbb{C}^{M\times K}$ and $\mathbf{G}^{dl} \in \mathbb{C}^{K\times M}$ are the channel matrices, respectively. The $\mathbf{P} \in \mathbb{C}^{M\times K}$ is the physical MIMO channel matrix with reciprocity and $\mathbf{B} = \mathrm{diag}(B_1, ..., B_M)$, $\mathbf{F} = \mathrm{diag}(F_1, ..., F_K)$ are the diagonal frequency response matrices at the AP and UE sides. Therefore, the following formulation can be derived: $g_{mk}^{dl} = \dfrac{F_K^{dl} B_M^{dl}}{F_K^{ul} B_M^{ul}} g_{mk}^{ul}$.

Similar to [3], [14], the physical propagation channels are modeled as $p_{mk} = \sqrt{\beta_{mk}} h_{mk}$, where β_{mk} denotes the large-scale fading coefficient while h_{mk} is the small-scale fading. All the h_{mk} are independent and identically distributed (i.i.d.) random variables (RVs) with $h_{mk} \sim \mathcal{CN}(0, 1)$ based on our assumption.

The statistics of $\mathbf{B}$ and $\mathbf{F}$ capture the randomness of the transceivers. And the phase and amplitude responses are independent for modeling purposes, thus B_m and F_k are respectively expressed as

$$\begin{aligned} B_m^x &= A_{B_m}^x e^{j\theta_{B_m}^x}, \\ F_k^x &= A_{F_k}^x e^{j\theta_{F_k}^x}, \end{aligned} \tag{1}$$

where A and θ denote the values of the amplitude and the phase responses, respectively, with $x \in \{ul, dl\}$.

III. Performance Analysis

A. Uplink Channel Estimation

Different from the propagation channel variations, the corresponding transceiver frequency responses generally vary considerably slowly in time, thus $\mathbf{B}$ and $\mathbf{F}$ can be reasonably assumed constant. Therefore, the power gains UL and DL channels are defined as [14], [19]:

$$\Omega_{mk}^{ul} \triangleq \mathbb{E}\left\{\left|g_{mk}^{ul}\right|^2\right\} = \left|F_k^{ul}\right|^2 \left|B_m^{ul}\right|^2 \cdot \beta_{mk}, \tag{2}$$

$$\Omega_{mk}^{dl} \triangleq \mathbb{E}\left\{\left|g_{mk}^{dl}\right|^2\right\} = \left|F_k^{dl}\right|^2 \left|B_m^{dl}\right|^2 \cdot \beta_{mk}, \tag{3}$$

and Ω_{mk}^{ul} is assumed to be known when computing below the UL MMSE channel estimate.

In the uplink training phase, all K UEs send pilots to the APs in the same time to estimate the channel. We denote the pilot sequence of the coherence interval (in samples) by τ_p, and let $\sqrt{\tau_p}\boldsymbol{\varphi}_k \in \mathbb{C}^{\tau_p \times 1}$ where $||\boldsymbol{\varphi}_k||^2 = 1$, be the pilot sequence used by the k-th UE.Then, the $\tau_p \times 1$ received pilot signal samples at the m-th AP is set as [3]:

$$\mathbf{y}_{p,m} = \sqrt{\tau_p \rho_u} \sum_{k=1}^{K} g_{mk}^{ul} \boldsymbol{\varphi}_k + \mathbf{w}_{p,m}, \tag{4}$$

where ρ_u is the uplink normalized signal-to-noise ratio (SNR) of each pilot symbol and $\boldsymbol{w}_{p,m}$ are i.i.d. $\mathcal{CN}(0, 1)$ RVs representing thermal noise at the m-th AP. To obtain samples proportional to the channel between the k-th UE and the m-th AP, thus the projection of $\mathbf{y}_{p,m}$ onto $\boldsymbol{\varphi}_k^H$ is given as:

$$\begin{aligned} \check{y}_{p,mk} &= \boldsymbol{\varphi}_k^H \mathbf{y}_{p,m} \\ &= \sqrt{\tau_p \rho_u} g_{mk}^{ul} + \sqrt{\tau_p \rho_u} \sum_{k' \neq k}^{K} g_{mk}^{ul} \boldsymbol{\varphi}_k^H \boldsymbol{\varphi}_{k'} + \boldsymbol{\varphi}_k^H \mathbf{w}_{p,m}. \end{aligned} \tag{5}$$

Then the MMSE estimate of g_{ul}^{mk} could be denoted as:

$$\begin{aligned} \hat{g}_{mk}^{ul} &= \frac{\mathbb{E}\left\{\check{y}_{\mathrm{p},mk}^* g_{mk}^{ul}\right\}}{\mathbb{E}\left\{\left|\check{y}_{\mathrm{p},mk}\right|^2\right\}} \check{y}_{p,mk} \\ &= \frac{\sqrt{\tau_u \rho_u} \Omega_{mk}^{ul}}{\tau_u \rho_u \sum_{k'=1}^{K} \Omega_{mk'}^{ul} \left|\boldsymbol{\varphi}_k^H \boldsymbol{\varphi}_{k'}\right| + 1} \check{y}_{p,mk}. \end{aligned} \tag{6}$$

Owing to the second term in (5), the pilots transmitted from other UEs degrade the channel estimate $\hat{g}_{mk}$, which causes the so-called pilot contamination.

B. Downlink Data Transmission

Let q_k denote the symbol prepared for the k-th UE with $\mathbb{E}\left\{\left|q_k\right|^2\right\} = 1$. And each q_k is accessible to the CPU for LSFP, following the previous literature [16]. In the first step, the CPU uses long-term statistics of the channel to conduct LSFP for the symbols transmitted from each AP. We denote a_{mk}^* as the complex weight applied to the data symbol of k-th

$$\mathrm{SINR}_k = \frac{\rho_d \left| \sum_{m=1}^{M} \left(a_{mk}\right)^* \gamma_{mk} \frac{F_k^{dl} B_m^{dl}}{F_k^{ul} B_m^{ul}} \right|^2}{\rho_d \sum_{k' \neq k}^{K} \left(\sum_{m=1}^{M} a_{mk'}^* \gamma_{mk'} \frac{\Omega_{mk}^{dl}}{\Omega_{mk'}^{dl}} \right)^2 \left| \varphi_{k'}^H \varphi_k \right|^2 + \rho_d \sum_{m=1}^{M} \Omega_{mk}^{dl} \sum_{k'=1}^{K} \left(a_{mk'}^*\right)^2 \gamma_{mk'} + 1}. \tag{20}$$

UE for the transmission of the combined signal v_{mk} from the m-th AP, i.e.

$$v_{mk} = a_{mk}^* q_k, \tag{7}$$

where v_{mk} is transmitted from m-th AP to the k-th UE as the precoding signal.

In the second step, the CPU sends the precoded symbols v_{mk} to the m-th AP. Since the LSFP coefficients a_{mk} can represent the power control coefficients, there is no need for additional localized power control coefficients at the APs.

In the last step, relying on NRC, the APs use the uplink channel estimates to estimate the downlink channel and compute local precoding, based on the channel information obtained from the uplink pilot transmission. The conjugate beamforming is used to send signals to the K UEs, the signal transmitted from the m-th AP is defined as follows:

$$x_m = \sqrt{\rho_d} \sum_{k=1}^{K} a_{mk}^* \hat{g}_{mk}^{*ul} q_k, \tag{8}$$

where ρ_{d} is the normalized downlink signal-to-noise ratio (SNR). The corresponding received signal at the k-th UE is

$$\begin{aligned} r_k =& \sqrt{\rho_d} \sum_{m=1}^{M} g_{mk}^{dl} x_m + w_k \\ =& \sqrt{\rho_d} \sum_{m=1}^{M} a_{mk}^* g_{mk}^{dl} \hat{g}_{mk}^{*ul} q_k \\ &+ \sqrt{\rho_d} \sum_{m=1}^{M} \sum_{k' \neq k}^{K} a_{mk'}^* g_{mk}^{dl} \hat{g}_{mk'}^{*ul} q_{k'} + w_k, \end{aligned} \tag{9}$$

where $w_k \sim \mathcal{CN}(0,1)$ denotes additive receiver thermal noise at the k-th UE.

Based on the channel hardening effect [3], [6], i.e., UEs only use the statistics of the beamformed channel to detect the desired symbol. The signal received by k-th UE in (9) is denoted as:

$$r_k = \mathrm{DS}_k + \mathrm{BU}_k + \mathrm{IUI}_k + w_k, \tag{10}$$

where

$$\mathrm{DS}_k = \sqrt{\rho_d} \mathbb{E} \left\{ \sum_{m=1}^{M} a_{mk}^* g_{mk}^{dl} \hat{g}_{mk}^{*ul} \right\} q_k, \tag{11}$$

$$\begin{aligned} \mathrm{BU}_k =& \sqrt{\rho_d} \left(\sum_{m=1}^{M} a_{mk}^* g_{mk}^{dl} \hat{g}_{mk}^{*ul} \right. \\ & \left. - \mathbb{E} \left\{ \sum_{m=1}^{M} a_{mk}^* g_{mk}^{dl} \hat{g}_{mk}^{*ul} \right\} \right) q_k, \end{aligned} \tag{12}$$

$$\mathrm{IUI}_k = \sqrt{\rho_d} \sum_{m=1}^{M} \sum_{k' \neq k}^{K} a_{mk'}^* g_{mk}^{dl} \hat{g}_{mk'}^{*ul} q_{k'}, \tag{13}$$

represent the strength of the desired signal (DS), the beamforming gain uncertainty (BU), and the inter-user interference resulted from the k-th UE (IUI), correspondingly. The sum of the second to fourth terms in (10) are defined as effective noise. According to [3], the DS and the effective noise are uncorrelated, which matches the so-called Use-and-then-Forget (UatF) [20]. In that case, we get the SE of the k-th UE [20]

$$\mathrm{SE}_k = \log_2(1 + \mathrm{SINR}_k), \tag{14}$$

where SINR_k, in our assumption, is given by

$$\mathrm{SINR}_k = \frac{\mathbb{E}\left\{ \left| \mathrm{DS}_k \right|^2 \right\}}{\mathbb{E}\left\{ \left| \mathrm{BU}_k \right|^2 \right\} + \mathbb{E}\left\{ \left| \mathrm{IUI}_k \right|^2 \right\} + 1}. \tag{15}$$

Using a similar approach as in [3], the three terms are separately computed as follows:

$$\mathbb{E}\left\{ \left| \mathrm{DS}_k \right|^2 \right\} = \rho_d \left| \sum_{m=1}^{M} a_{mk}^* \gamma_{mk} \frac{F_k^{dl} B_m^{dl}}{F_k^{ul} B_m^{ul}} \right|^2, \tag{16}$$

$$\mathbb{E}\left\{ \left| \mathrm{BU}_k \right|^2 \right\} = \rho_d \sum_{m=1}^{M} \left(a_{mk}^*\right)^2 \Omega_{mk}^{dl} \gamma_{mk}, \tag{17}$$

$$\begin{aligned} \mathbb{E}\left\{ \left| \mathrm{IUI}_k \right|^2 \right\} =& \rho_d \sum_{m=1}^{M} \Omega_{mk}^{dl} \sum_{k' \neq k}^{K} \left(a_{mk'}^*\right)^2 \gamma_{mk'} \\ &+ \rho_d \sum_{k' \neq k}^{K} \left(\sum_{m=1}^{M} a_{mk'}^* \gamma_{mk'} \frac{\Omega_{mk}^{dl}}{\Omega_{mk'}^{dl}} \right)^2 \left| \varphi_{k'}^H \varphi_k \right|^2, \end{aligned} \tag{18}$$

where

$$\gamma_{mk} \triangleq \mathbb{E}\left\{ \left| \hat{g}_{mk}^{ul} \right|^2 \right\} = \frac{\tau_u \rho_u \left(\Omega_{mk}^{ul}\right)^2}{\tau_u \rho_u \sum_{k'=1}^{K} \Omega_{mk'}^{ul} \left| \boldsymbol{\varphi}_k^H \boldsymbol{\varphi}_{k'} \right| + 1}. \tag{19}$$

The final formulation of the effective SINR, including both the effects of the uplink-based channel estimation and the NRC, is shown at the top of the last page as (20).

C. Impact of Non-Reciprocity With Perfect CSI and Pilot Contamination

In this section, we discuss the AP-side perfect CSI to simplify the closed-form expressions, and to focuses on the effects of the NRC alone. Thus the uplink channel estimate power is denoted by $\gamma_{mk} = \Omega_{mk}^{ul}$, while the DS power and

the SI plus IUI power are given by

$$\mathbb{E}\left\{\left|\mathrm{DS}_k\right|^2\right\} = \rho_d \left|F_k^{ul}\right|^2 \left|F_k^{dl}\right|^2 \left|\sum_{m=1}^{M} a_{mk}^* \beta_{mk} \frac{\left|B_m^{ul}\right|^2}{B_m^{ul}} B_m^{dl}\right|^2, \tag{21}$$

$$\begin{aligned}&\mathbb{E}\left\{\left|\mathrm{BU}_k\right|^2\right\} + \mathbb{E}\left\{\left|\mathrm{IUI}_k\right|^2\right\} \\ &= \rho_d \sum_{m=1}^{M} \left|F_k^{dl}\right|^2 \left|B_m^{dl}\right|^2 \beta_{mk} \sum_{k'=1}^{K} \left(a_{mk'}^*\right)^2 \left|F_{k'}^{ul}\right|^2 \left|B_m^{ul}\right|^2 \beta_{mk'} \\ &+ \rho_d \sum_{k' \neq k}^{K} \left(\sum_{m=1}^{M} a_{mk'}^* \frac{\left|F_{k'}^{ul}\right|^2 \left|B_m^{ul}\right|^2 \left|F_k^{dl}\right|^2}{\left|F_{k'}^{dl}\right|^2} \beta_{mk}\right)^2 \left|\varphi_{k'}^H \varphi_k\right|^2.\end{aligned} \tag{22}$$

1) Analysis for UE Side NRC: From (21) and (22), we note that only amplitude response at UEs appears in the expressions, thus the UE-side phase NRC shows no effect on the downlink SE. Moreover, we can observe that the interference terms in (22) are all the product of the transceiver frequency responses, thus the UE-side NRC shows no effect on the interference power. Furthermore, in (21), the amplitude NRC disappeared due to the product of amplitude responses in both uplink and downlink, thus such NRC shows no reduction the beamforming gain. Therefore, the UE-side NRC shows no effect the system performance.

2) Analysis for AP Side NRC: Based on (21), B_m is normalized in amplitude. Thus the AP-side amplitude mismatch will not reduce the beamforming gain. But the AP-side phase non-reciprocity will affect the beamforming direction, reducing the beamforming gain. Since only the product of the transceiver frequency responses is contained in (22), the NRC will not increase the IUI power.

Thus we can derive that only the AP-side phase NRC reduces the performance, which is similar to the conclusion in [14]. This paper expands such conclusion to random pilot contamination, which makes it work at a more common statement.

IV. Max-Min Power Control

The radio resources should be managed considerably to get good system performance. In this section, we derive a power control algorithm based on the NRC to maximize the service of the weakest UE. And importantly, the power control is done on the large-scale fading time scale and CPU. However, the NRC will not happen at the uplink, thus only the power control in the downlink is considered by us.

For the given large-scale fading, the LSFP coefficients $a_{mk}^*, m = 1, ..., M, k = 1, ..., K$ will maximize the downlink SE of the weakest UE, under the constraint: $\mathbb{E}\left\{\left|x_m\right|^2\right\} \leq \rho_d$. With the channel model we defined, the power constraint could be rewritten as:

$$\sum_{k=1}^{K} \left(a_{mk}^*\right)^2 \gamma_{mk} \leq 1, m = 1, ..., M. \tag{23}$$

Then the max-min power control strategy is defined mathematically:

$$\begin{aligned}&\max_{\left\{a_{mk}^*\right\}} \min_{k=1,...,K} \mathrm{SE}_k \\ &\text{subject to} \\ &\sum_{k=1}^{K} \left(a_{mk}^*\right)^2 \gamma_{mk} \leq 1, m = 1, ..., M \\ &a_{mk} \geq 0, m = 1, ..., M, k = 1, ..., K,\end{aligned} \tag{24}$$

where SE_k is $\log_2\left(1 + \mathrm{SINR}_k\right)$.

After introducing slack variables θ_m and $\varrho_{k'k}$, the formula can be expressed as follows:

$$\begin{aligned}&\max_{\left\{a_{mk}^*, \theta_m, \varrho_{k'k}\right\}} \min_{k=1,...,K} \\ &\frac{\left|\sum_{m=1}^{M} \left(a_{mk}\right)^* \gamma_{mk} \frac{F_k^{dl} B_m^{dl}}{F_k^{ul} B_m^{ul}}\right|^2}{\sum_{k' \neq k}^{K} \left|\varphi_{k'}^H \varphi_k\right|^2 \varrho_{k'k}{}^2 + \sum_{m=1}^{M} \Omega_{mk}^{dl} \theta_m^2 + \frac{1}{\rho_d}} \\ &\text{subject to} \\ &\sum_{k=1}^{K} \left(a_{mk'}^*\right)^2 \gamma_{mk'} \leq \theta_m^2, m = 1, ..., M \\ &\sum_{m=1}^{M} a_{mk'}^* \gamma_{mk'} \frac{\Omega_{mk}^{dl}}{\Omega_{mk'}^{dl}} \leq \varrho_{k'k}, \forall k' \neq k \\ &a_{mk} \geq 0, m = 1, ..., M, k = 1, ..., K.\end{aligned} \tag{25}$$

Lemma 1. *The objective function and the problem in (25) are all quasi-concave.*

Proof: It follows similar steps in [3, Appendix B]. The upper-level set of the objective function in (25) can be represented as a second-order cone (SOC), it is a convex set. Thus, the objective function in (25) is quasi-concave. Since the constraint set in (25) is also convex, the optimization problem (25) is a quasi-concave optimization problem. ■

In the following, we use a bisection search to solve (25), where a sequence of convex feasibility problems is solved in every step. Specifically, Algorithm 1 is proposed to solve the problems.

V. Numerical Results

A. Large-Scale Fading Model and Simulation Setup

Next, we consider a network where 100 APs and 40 UEs are evenly distributed at random over a square of size 1×1 km^2 at 1.9 GHz. The large-scale fading coefficient β_{mk} is modeled using the three-slope model [3]. All parameters are collected in Table I.

To get reproducible results, we set $\left\{A_{F_k}^{ul}, A_{F_k}^{dl}, A_{B_m}^{ul}, A_{B_m}^{dl}\right\}$ as uniform random variables from $1 - \epsilon$ to $1 + \epsilon$. And we choose ϵ to make $\sigma_A^2 = 0.01$. We make $\left\{\theta_{F_k}^{ul}, \theta_{F_k}^{dl}, \theta_{B_m}^{ul}, \theta_{B_m}^{dl}\right\}$ distributed from $-\pi$ to π uniformly.

Algorithm 1: Bisection Algorithm for Solving (25)

1 Initiation: choose two initial values t_{max} and t_{min} that decide the range of relevant values in objective function in (25). Choose a positive tolerance ϵ.

2 Let $t = \frac{t_{max}+t_{min}}{2}$ and solve the convex feasibility program as follows:

$$\begin{aligned} &\mathrm{SINR}_k \geq t, k = 1, ..., K, \\ &\sum_{k=1}^{K} \left(a^*_{mk'}\right)^2 \gamma_{mk'} \leq \theta^2_m, m = 1, ..., M, \\ &\sum_{m=1}^{M} a^*_{mk'} \gamma_{mk'} \frac{\Omega^{dl}_{mk}}{\Omega^{dl}_{mk'}} \leq \varrho_{k'k}, \forall k' \neq k, \\ &a_{mk} \geq 0, m = 1, ..., M, k = 1, ..., K. \end{aligned} \tag{26}$$

3 if (26) is feasible, let $t_{min} = t$, otherwise, let $t_{max} = t$.

4 if $t_{max} - t_{min} < \epsilon$, stop, else turn back to Step 2.

TABLE I
SYSTEM PARAMETERS.

Parameters	Values
Centre frequency	1.9 GHz
M	100
K	40
UL pilot length	20
Bandwidth	20MHz
Noise figure	9db
AP antenna height	15 m
UE antenna height	1.65 m
$\rho_{\mathrm{d}}, \rho_{\mathrm{p}}$	200,100mW

B. Results and Discussions

First, the effect of NRC and the pilot contamination are compared on the SE of the UEs. Since pilot contamination is unlimited, it cannot be compared with NRC directly. However, due to the common view in CF massive MIMO that $M >> K$, we set the upper bound of K to twice the number of orthogonal pilots. Thus NRC and pilot contamination can be compared at the same scale.

Fig. 2 shows the per-user SE in different root mean squared error (RMSE) of frequency responses of APs and the number of UEs, which represent the degree of channel reciprocity and degree of pilot contamination respectively. The 20 and 40 are the lower bound and upper bound of K, while 0 and 104 are the Lower bound and upper bound of RMSE. To find which fator affects the donwlink SE more, we set the RMSE of frequency responses of APs at the midpoint, i.e., 52, and change the K from 20 to 40. Similarly, we set the K to 30 and change the RMSE of frequency responses of APs from 0 to 104°. Under the equal power control scheme, the drop of per-user SE from pilot contamination changes 0.48 more than NRC. However, we find a more interesting character of NRC relying on the following analysis.

Furthermore, the CDFs of per-user SE for different kinds

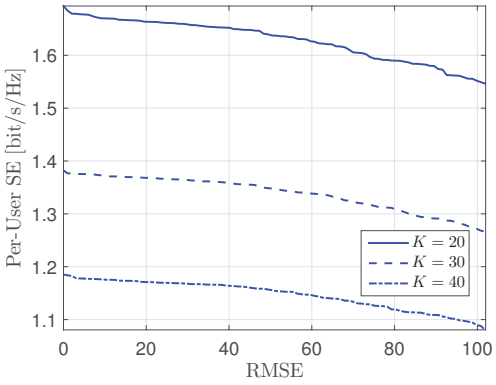

Fig. 2. Per-User SE against different RMSE of frequency responses of APs and the number of UEs.

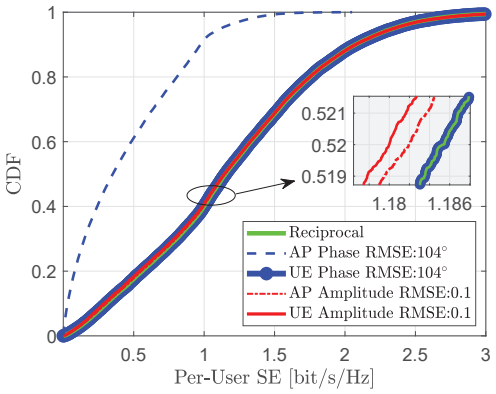

Fig. 3. CDFs for the per-user SE against different non-reciprocity sources.

of NRC sources are compared in Fig. 3, and other sources disappear. When NRC is considered, transceiver frequency responses are uncorrelated in these evaluations. The result shows that the downlink SE is only affected by AP-side phase NRC, which confirms the conclusion obtained from the analysis in Section III.

In Figs. 4 and 5, the CDFs of per-user SE between the max-min power control and without power control, i.e., equal power control, are compared in different NRC degrees. In Fig. 4, the RMSE of frequency responses of APs is set to 30.4 while in Fig. 5 it is 104. We observe that when the NRC degree is low, the max-min power control performs better than equal power control. However, when the NRC degree is high, the max-min power control provides negligible gain among the UEs that have the weakest SE while reducing the SE of other UEs largely. Such a conclusion is different from the obvious research [3], [21], [22]. The result is decided by the property of the max-min power control itself, which just focuses on the weakest UE while ignoring the others, this makes it unable to guarantee the excellent overall power of all UEs. Since the DS is the sum of the complex signal, which is caused by AP-side frequency responses, the received signal is canceled with each other. This makes the weakest UE difficult to improve SE. The max-min power control should be used only when the NRC

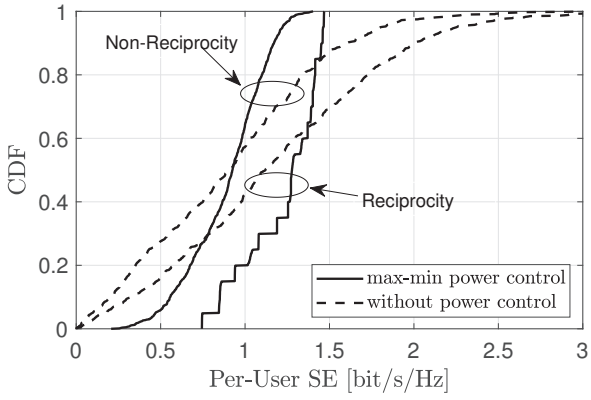

Fig. 4. CDFs of per-user SE with and without the max-min power control. (RMSE of frequency responses of APs is 30.4°).

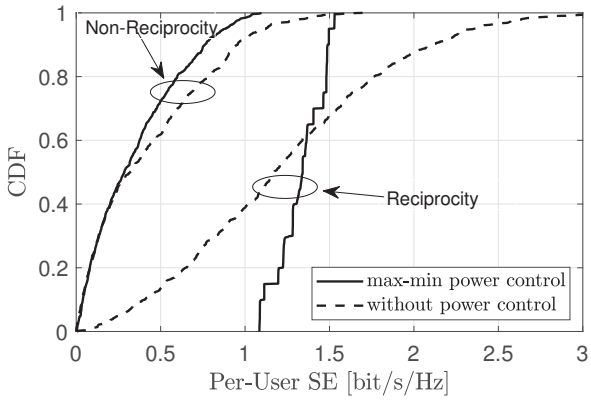

Fig. 5. CDFs of per-user SE with and without the max-min power control. (RMSE of frequency responses of APs is 104°).

degree is low due to the poor performance of UEs.

VI. Conclusion

This paper analyzed the performance of CF massive MIMO systems with conjugate beamforming for both perfect and imperfect channel estimation, considering the physically slow-varying NRC and pilot contamination. We compared the effect of NRC and the pilot contamination in CF massive MIMO systems. More importantly, we take into account the effects of NRC in max-min power control. Under our analysis, only the AP-side phase errors affect the downlink SE of the system with pilot contamination. Under the equal power scheme, the pilot contamination shows a greater effect on the downlink SE than NRC. However, The performance of the power control scheme shows sensitivity to NRC. In particular, the max-min power control will lose its superiority as the AP-side phase error increases. These observations are fresh and different from the extant CF research considering perfect NRC and indicate that the choice of power control scheme must consider the effect of NRC. Extending such analysis to other power control and precoding schemes should be important topics for future work.

References

[1] J. Zhang, E. Björnson, M. Matthaiou, D. W. K. Ng, H. Yang, and D. J. Love, "Prospective multiple antenna technologies for beyond 5G," *IEEE J. Sel. Areas Commun*, vol. 38, no. 8, pp. 1637–1660, Aug. 2020.

[2] E. Nayebi, A. Ashikhmin, T. L. Marzetta, H. Yang, and B. D. Rao, "Precoding and power optimization in cell-free massive MIMO systems," *IEEE Trans. Wireless Commun.*, vol. 16, no. 7, pp. 4445–4459, Jul. 2017.

[3] H. Q. Ngo, A. Ashikhmin, H. Yang, E. G. Larsson, and T. L. Marzetta, "Cell-free massive MIMO versus small cells," *IEEE Trans. Wireless Commun.*, vol. 16, no. 3, pp. 1834–1850, Mar. 2017.

[4] J. Zheng, J. Zhang, and B. Ai, "UAV communications with WPT-aided cell-free massive MIMO systems," *IEEE J. Sel. Areas Commun.*, to appear, 2021.

[5] H. Liu, J. Zhang, S. Jin, and B. Ai, "Graph coloring based pilot assignment for cell-free massive MIMO systems," *IEEE Trans. Veh. Technol.*, vol. 69, no. 8, pp. 9180–9184, Aug. 2020.

[6] H. Q. Ngo and E. G. Larsson, "No downlink pilots are needed in TDD massive MIMO," *IEEE Trans. Wireless Commun.*, vol. 16, no. 5, pp. 2921–2935, May 2017.

[7] S. Chen, J. Zhang, E. Björnson, J. Zhang, and B. Ai, "Structured massive access for scalable cell-free massive MIMO systems," *IEEE J. Sel. Areas Commun.*, vol. 39, no. 4, pp. 1086–1100, Apr. 2021.

[8] Ö. Özdogan, E. Björnson, and J. Zhang, "Performance of cell-free massive MIMO with Rician fading and phase shifts," *IEEE Trans. Wireless Commun.*, vol. 18, no. 11, pp. 5299–5315, Nov. 2019.

[9] D. Mi, M. Dianati, L. Zhang, S. Muhaidat, and R. Tafazolli, "Massive MIMO performance with imperfect channel reciprocity and channel estimation error," *IEEE Trans. Commun.*, vol. 65, no. 9, pp. 3734–3749, Sep. 2017.

[10] J. Zheng, J. Zhang, E. Björnson, and B. Ai, "Impact of channel aging on cell-free massive MIMO over spatially correlated channels," *IEEE Trans. Wireless Commun.*, to appear, 2021.

[11] Z. Wang, J. Zhang, E. Björnson, and B. Ai, "Uplink performance of cell-free massive MIMO over spatially correlated Rician fading channels," *IEEE Commun. Lett.*, vol. 25, no. 4, pp. 1348–1352, Apr. 2020.

[12] R. Rogalin, O. Y. Bursalioglu, H. Papadopoulos, G. Caire, A. F. Molisch, A. Michaloliakos, V. Balan, and K. Psounis, "Scalable synchronization and reciprocity calibration for distributed multiuser MIMO," *IEEE Trans. Wireless Commun.*, vol. 13, no. 4, pp. 1815–1831, Apr. 2014.

[13] O. Raeesi, A. Gokceoglu, and M. Valkama, "Estimation and mitigation of channel non-reciprocity in massive MIMO," *IEEE Trans. Signal Process.*, vol. 66, no. 10, pp. 2711–2723, May 2018.

[14] J. M. Palacios, O. Raeesi, A. Gokceoglu, and M. Valkama, "Impact of channel non-reciprocity in cell-free massive MIMO," *IEEE Wireless Commun. Lett.*, vol. 9, no. 3, pp. 344–348, Mar. 2019.

[15] A. A. Ohashi, D. B. da Costa, A. L. P. Fernandes, W. Monteiro, R. Failache, A. M. Cavalcante, and J. C. W. A. Costa, "Cell-Free Massive MIMO-NOMA Systems with Imperfect SIC and Non-Reciprocal Channels," *IEEE Wireless Commun. Lett.*, pp. 1–1, Mar. 2021.

[16] A. Ashikhmin, L. Li, and T. L. Marzetta, "Interference reduction in multi-cell massive mimo systems with large-scale fading precoding," *IEEE Trans. Inf. Theory*, vol. 64, no. 9, pp. 6340–6361, Jul. 2018.

[17] T. Van Chien, C. Mollén, and E. Björnson, "Large-scale-fading decoding in cellular massive MIMO systems with spatially correlated channels," *IEEE Trans. Commun.*, vol. 67, no. 4, pp. 2746–2762, Apr. 2019.

[18] O. Raeesi, A. Gokceoglu, Y. Zou, E. Björnson, and M. Valkama, "Performance analysis of multi-user massive MIMO downlink under channel non-reciprocity and imperfect CSI," *IEEE Trans. Commun.*, vol. 66, no. 6, pp. 2456–2471, Jun. 2018.

[19] Y. Jin, J. Zhang, S. Jin, and B. Ai, "Channel estimation for cell-free mmWave massive MIMO through deep learning," *IEEE Trans. Veh. Technol.*, vol. 68, no. 10, pp. 10 325–10 329, Oct. 2019.

[20] E. Björnson, J. Hoydis, and L. Sanguinetti, "Massive MIMO networks: Spectral, energy, and hardware efficiency," *in Foundations and Trends in Signal Processing*, vol. 11, no. 3-4, pp. 154–655, 2017.

[21] J. Zheng, J. Zhang, L. Zhang, X. Zhang, and B. Ai, "Efficient receiver design for uplink cell-free massive MIMO with hardware impairments," *IEEE Trans. Veh. Technol.*, vol. 69, no. 4, pp. 4537–4541, Apr. 2020.

[22] E. Björnson and L. Sanguinetti, "Making cell-free massive MIMO competitive with MMSE processing and centralized implementation," *IEEE Trans. Wireless Commun.*, vol. 19, no. 1, pp. 77–90, Jan. 2020.